CSCE Annual Conference

Growing with youth – Croître avec les jeunes

Laval (Greater Montreal)

June 12 - 15, 2019/ *12 – 15 Juin, 2019*

BOND BEHAVIOUR OF STEEL REINFORCING BARS EMBEDDED IN ULTRA-HIGH-PERFORMANCE STEEL FIBER REINFORCED CONCRETE

Saikali, E, Rita[1,3], Palermo, Dan[2] and Pantazopoulou, S.J.[2]

[1] MASc Candidate, Department of Civil Engineering, York University, Toronto, Canada

[2] Professor, Department of Civil Engineering, York University, Toronto, Canada

[3] ritasai@yorku.ca

Abstract: This paper presents results from an experimental study conducted to investigate the bond behavior of steel reinforcing bars embedded in Ultra-High-Performance Steel-Fiber-Reinforced Concrete (UHP-SFRC). UHP-SFRC is currently considered an optimal, durable material, which can be a substitute for conventional concrete owing to its distinct fresh and hardened properties. Thus, it is essential to understand the mechanism of stress transfer between UHP-SFRC and conventional reinforcement that permits the composite action of both materials. A four-point bending test program was conducted on 7 beams designed for the reinforcing bar development to occur in the constant moment region over a short embedment length to achieve as close as uniform distribution of bond stresses, enabling measurement of bond strength through inverse analysis of beam strength and deformation. Confinement was only provided by the concrete cover. Three design UHP-SFRC mixes were assessed: two commercial and one developed in-house with a compressive strength greater than 120 MPa after 120 days. The bond strength was observed to be directly proportional to the tensile strength of the mix, where for the strongest material the average bond strength reached 30 MPa. Moreover, the test results indicated a very ductile flexural beam response accompanied by significant mid-span deflections and substantial bar-slip. The bond-specimens failed either by pullout or by cone formation with minimal deterioration of the concrete cover, illustrating the high confinement provided by the concrete surrounding the bar. The yielding of the reinforcing bar illustrated that the high bond strength, provided by the concrete cover, enables significant reduction in the design development length as currently specified for conventional concrete.

1 INTRODUCTION

After exposure to severe climatic conditions, conventional reinforced concrete structures initially designed for service lives between 50 to 99 years require rehabilitation after 30 years of usage with an estimated yearly cost exceeding $1 billion for bridges and $20 billion for building structures (Kumar and Burrows 2001; Gürkan et al. 2018). UHP-SFRC has therefore been proposed as an optimal economic and innovative sustainable material to be used to retrofit several infrastructure projects in place of conventional concrete (Doiron 2017). In 2016, a research survey highlighted that 87 bridges in Canada were built using UHP-FRC (Haber et al. 2018).

Extremely high strength concrete was first developed using a very low porosity matrix. It was found that with vacuum mixing, it was possible to reach very high compressive strength up to 230 MPa, whereas, this strength could attain 680 MPa after heat treatment procedures (Yudenfreund et al. 1972; Roy et al. 1972). In the early 1980s, newly discovered pozzolans in the form of reactive powders and superplasticizer admixtures were added to reduce the porosity of normal weight concrete creating concretes known as Macro-Defect-Free (MDF) and Densified Small Particle (DSP) mixes (Bache 1981; Alford et al. 1982).

However, this material presented poor tensile strength with a brittle failure mode as shown in Figure 1 (a). The subsequent addition of fibers in the matrix enhanced the tension behavior of concrete found in Slurry Infiltrated Fiber Concrete (SIFCON) and Engineering Cementitious Composites (ECC) qualified as High-Performance-Fiber Reinforced concrete (HP-FRC) (Lankard 1985; Li and Leung 1992). Thereafter, UHP-FRC mixes were developed such as Reactive Powder Concrete (RPC) overcoming the performance of HP-FRC. This led to a very dense matrix designed with high homogeneity owing to the elimination of coarse aggregates, the reduction of porosity, and improvement of the microstructure with a water/binder ratio of 0.25. These improvements increased the compressive strength to greater than 150 MPa even when mixed at ambient temperatures (Richard and Cheyrezy 1995). The matrix contained short steel fibers in an optimal volumetric fraction of 2.5% to maintain an effective workability with a strong bond between the two materials. This fibre content resulted in a “strain-hardening” behavior in direct tension defined by the capability to develop multiple cracking after the development of the first crack and prior to the initiation of crack localization once the peak load was reached as depicted in Figure 1 (b) (Naaman and Reinhardt 2003).

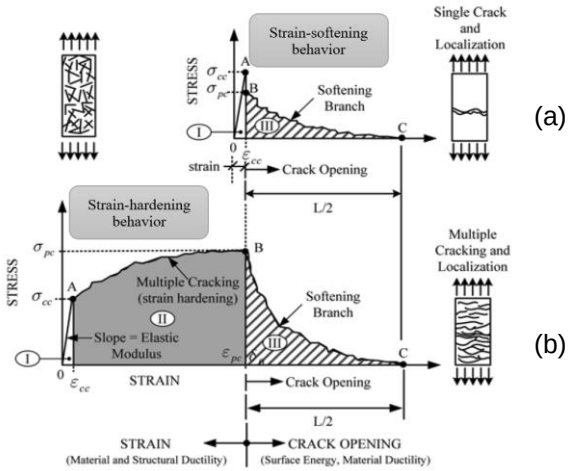

Figure 1: (a) Strain-softening and (b) strain-hardening behaviour (Naaman and Reinhardt 2003)

For the past two decades, the favorable mechanical properties of UHP-SFRC have been thoroughly identified. However, these distinct properties are not considered currently in structural design given that no appropriate design codes specific to this innovative concrete are available currently (Annex 8.1 of CHBDC is presently under development to address this need). An example is the required development length proposed in concrete design codes to develop the strength of the reinforcing bar: knowledge of the bond-stress and slip at the interface of steel reinforcement and UHP-SFRC is needed. In fact, deformed reinforcing bars subject to a tensile force tend to slip relative to the surrounding concrete where the bond strength is due to the capacity of the nearby concrete cover to carry hoop tension, exhibiting a force transfer mechanism that is defined by the local bond stress-slip relationship. For large bar slip, the stress transfer between the concrete and the steel is only ensured by the inclined bearing force which may be resolved for convenience to the bond force along the bar axis, and the radial compression forces (ACI Committee 408 2003). The radial stresses along the perimeter of the ribs create internal tensile hoop stresses shown in Figure 2 (a). Once the tensile strength of concrete is exceeded, longitudinal cracks start to appear resulting in a splitting failure mode of the system.

Tastani and Pantazopoulou (2010) revealed that adequate confining pressure applied externally can counteract the tensile hoop stresses leading to the delay or even elimination of the splitting failure mode. The increased pressure that would be sustained on the bar lateral surface would, in turn, support a larger longitudinal component marked eventually by a pure pullout mode of the bar with little or no splitting (Tastani and Pantazopoulou 2010). Steel fibers enhance the concrete matrix by bridging through the opening of cracks to ensure transfer of load. The fibres act mainly as confinement to prevent the concrete from

expanding and reaching its limit of incompressibility as shown in Figure 2 (b). This enables the reinforcing bar to accomplish its initial role.

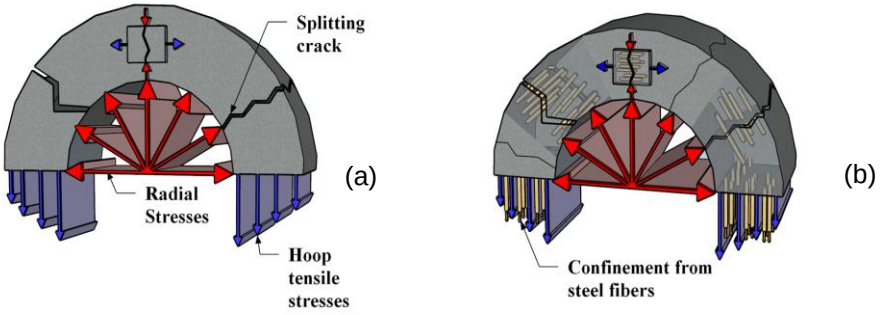

Figure 2: (a) Splitting crack and (b) multiple cracking due to fiber bridging

Three types of bond tests have been conducted previously on UHP-SFRC: standard pullout, direct splice pullout, and beam splice tests. For the standard pullout test, the bond strength was extremely high, reaching 60-80 MPa. Embedment lengths of 1.5 and $3d_b$ were required to eliminate rupture of the reinforcing bars and to promote a pullout-mode of failure (Schoening and Hegger 2012; Vitek et al. 2013). For the direct splice test, the bond strength was approximately 10-11 MPa and the specimens mainly failed by splitting cracks or yielding of the reinforcing bar (Lagier et al. 2016). Both tests demonstrated that the use of UHP-SFRC reduces the splice length required to develop the yield strength of the reinforcing bar. A Four-Point Bending Test (FPBT) was conducted with a splice length of $6d_b$ but failed by shear prior to bond due to the specimen detailing (Ronanki et al. 2016). Based on the authors' knowledge, no beam tests have been performed on reinforcing bar anchorage in UHP-SFRC to quantify bond.

The bond test setup of this study is based on Tastani et al. (2016) but considers longer beams and a different type of High-Performance Fiber-Reinforced-Concrete. The research presented herein offers an understanding of the experimental bond-stress-slip relationship for the "steel UHP-SFRC" system to explore the contribution of the tensile strength of UHP-SFRC on the development of steel reinforcing bars. Three different mixes were selected to study a range of UHP-SFRC materials and to identify the effect of the mechanical properties of each mixture on bond strength. The paper presents the experimental bond-stress-slip relationship obtained from a FPBT, where a direct linear relationship between the flexural tensile strength of the mixture and the bond strength was observed.

2 EXPERIMENTAL PROGRAM

2.1 Specimen detailing and setup

Seven beam specimens were tested in a four-point loading arrangement. The beams were 914 mm long with a 152 mm x 152 mm square cross section. The length of the beam was constructed to be 14 mm shorter than the length of the formwork to permit an extension of the primary steel bar for slip measurement. The 900 mm long beams were simply supported and subject to two equal and symmetrical loads spaced at 200 mm, creating a constant moment region between the loading points. No shear reinforcement was necessary in the constant moment region. The beams were designed for a flexural shear span of 300 mm. Lastly, the beams extended approximately 50 mm beyond the supports. Moreover, 15M steel bars were chosen for this study. The nominal yield strength and ultimate strength of these reinforcing bars are 400 MPa and 600 MPa, respectively. As shown in Figure 3, the embedment length was located in the constant moment region along a short length of $5d_b$ (80 mm) where the bond stress is expected to be nearly uniform. The concrete cover was a parameter of study. This enabled evaluating the contribution of the tensile properties of the concrete cover in resisting the tensile hoop stresses as the sole source of confinement. Arching action is not a concern here because the test bar is not anchored in the right hand side shear span.

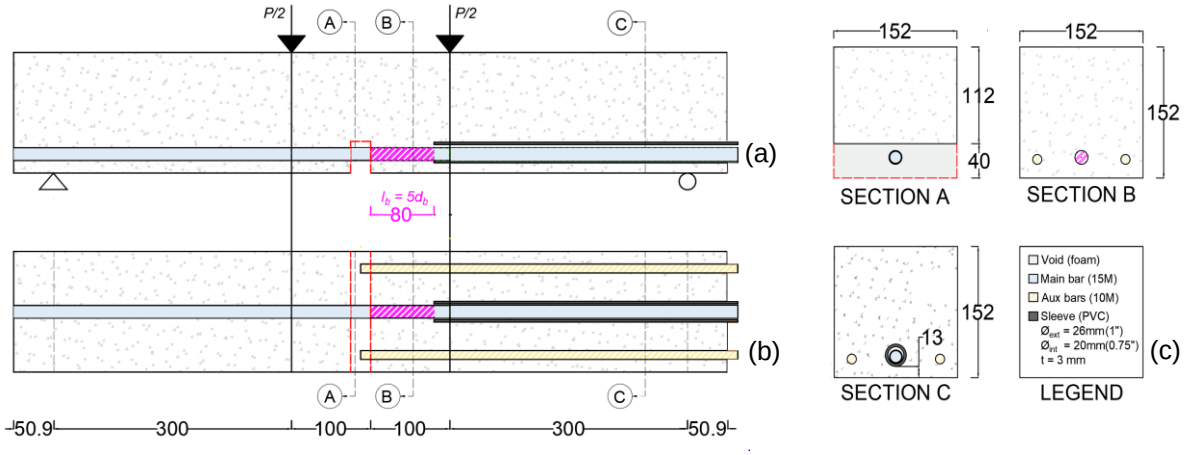

Figure 3: Specimen detailing: (a) front view, (b) top view and (c) cross-sections (all dimensions in mm)

As depicted in Figure 4, the desired embedment length was attained by covering the reinforcing bar with a PVC pipe (polyvinyl chloride) on the right side and a foam board on the left side. The main purpose of the foam board was to form a notch adjacent to the studied embedment length and to isolate the bar from the surrounding concrete. The notch enabled back calculation, through global equilibrium of the specimen, of the bar forces that were developed through bond over the studied bonded length. In addition, two auxiliary 10M bars were placed on both sides of the main bar to prevent premature flexural failure of the specimens before bond failure, which was the objective of this study. To isolate the 15M bar from the surrounding concrete, the height of the notch was set at 40 mm so it would exceed the combined height of the concrete cover and bar diameter.

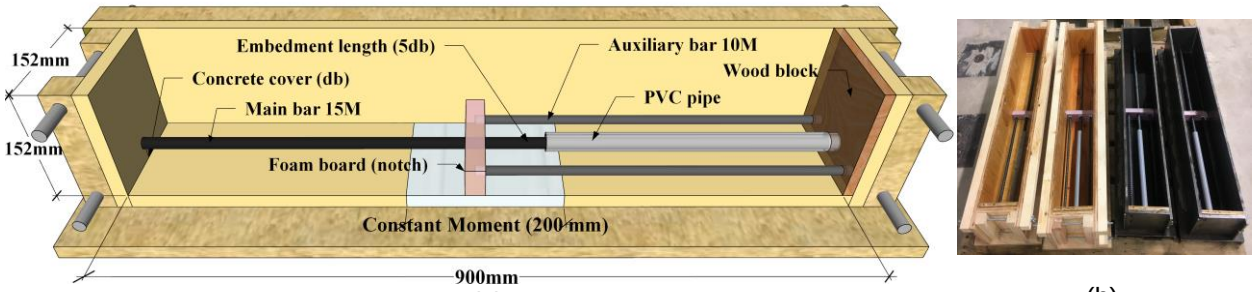

Figure 4: (a) Beam setup detailing and (b) prepared formwork

2.2 Test-setup and instrumentation

A static hydraulic universal test system was used to impose a displacement-controlled rate of 0.005 mm/min on the specimens. As shown in Figure 5 two linear potentiometers A and B were mounted to the specimens and connected to a data acquisition system to record during testing the vertical and horizontal displacements, respectively. The data were recorded at a frequency of 1 Hz, and the test was terminated once the peak load dropped by 80%. During testing, the applied load, mid-span deflection, and slip of the reinforcing bar were measured. Cracking and the mode of failure were also observed and analyzed. Assuming a uniform distribution of the bond stress along the embedment length, the average bond stress, f_b, was calculated at the loaded end of the reinforcing bar using Equation 1:

$$[1] \quad f_b = \frac{d_b * f_s}{4 * l_b}$$

where f_s is the bar stress calculated from sectional analysis of the beam at the notch, d_b is the nominal bar diameter and l_b is the embedment length.

Figure 5 (a) presents the back of the test setup. A frame chord system was pinned to the beam, providing pin-roller support to the aluminum bar (the chord) which carried linear potentiometer A to measure the mid-span deflection from the beam top compression fiber while excluding the rotation of the supports. Figure 5 (b) presents the frame that was fixed to the end of the beam holding the linear potentiometer B directly in contact with the extended end of the 15M bar to obtain slip measurements. The frame followed the movement of the beam eliminating the effect of the rotation of the supports from the slip measurement. The Digital Image Correlation (DIC) method was also conducted using GeoPIV-RG software, programmed within Matlab to calculate the mid-span deflection of a beam at the desired point (White et al. 2003).The software, based on localizing the centroid of a small group of pixels, uses an initial picture captured at the beginning of the test as a point of reference. Then, it determines the movement of this centroid, varying according to the timing of the images placed in sequence, thereby enabling the calculation of relative translations and strains. The cameras were placed facing the front side of the test setup. The (DIC) results were compared with the results obtained from the linear potentiometer.

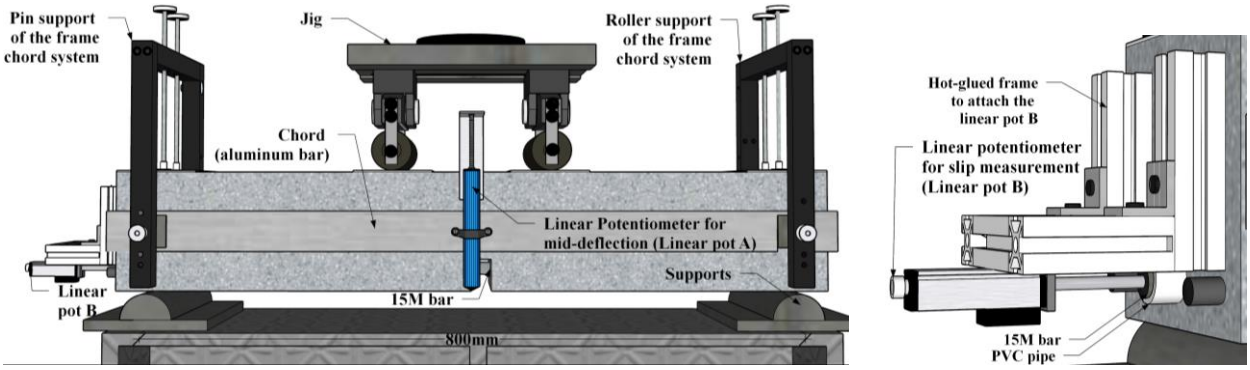

(a) (b)

Figure 5: (a) Test setup with linear potentiometer A for mid-deflection and (b) frame for linear potentiometer B for slip measurement

2.3 Test matrix characteristics

2.3.1 Design proportions and casting

The In-house mix was based on a previously developed design mixture (Shao 2016), slightly modified to obtain an adequate flowability and is presented in Table 1. In addition, the research included specimens cast using two proprietary concrete commercial design mixes denoted Com K and Com F. The In-house UHP-FRC contains a volumetric fraction of 2.5% brass-coated steel fibers (13 mm long and 0.2 mm diameter) and a water-to-binder ratio of 0.2. Com K contained 2% of identical steel fibers used in the In-house design mixture, while Com F contained 1% straight steel fibers (19 mm long and 0.2 mm diameter) and 1% hooked end steel fibers (25 mm long and 0.3 mm diameter).

Table 1: Proportions for the In-house design mixture

Cement (kg/m^3)	Fine Sand (kg/m^3)	Slag (kg/m^3)	Silica Fume (kg/m^3)	Superplasticizer (kg/m^3)	Water (kg/m^3)	Steel Fibers (kg/m^3)	w/b
724.13	668.6	362.06	120.69	11.1	241.13	195.75	0.2

The flow test results based on (ASTM C1856 2017) for the In-house design mixture and on (ASTM-C230 2010) for the commercial mixes, were about 210 mm for each mix. The casting procedure was based on (ASTM C1856 2017) following a layered method of pouring as shown in Figure 6 (a). The specimens were demolded two days after casting and stored in ambient laboratory temperature, covered with wet burlap sheets and a vapour barrier. The specimens were replicated 2-3 times, and the similarity in the response illustrated the accuracy, and repeatability of the experimental tests. Figure 6 (b) presents the prepared

specimens where a high strength gypsum plaster was placed on top to even and flatten the surface (USG Plasters). The bottom face of the specimen was painted white to detect the onset of cracking. To perform an image correlation on the flexural prisms and bond beams, a white inelastic primer was used as a base coat then speckled with black, white and pink dots.


(a)

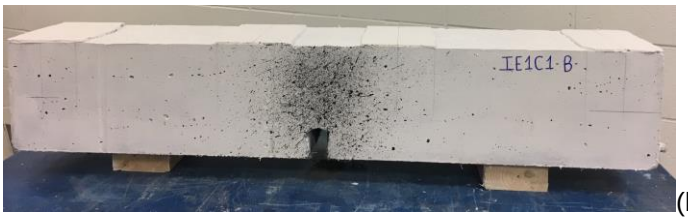

(b)

Figure 6: (a) Casting and (b) preparation of the test specimens

The specimen identification code comprises three parts. The first digit refers to the first initial of the concrete mix: K for the Com K's mix, F for the Com F's mix or I for the In-house design mix. The second and third digit, E1, corresponds to the embedment length of $5d_b$. The fourth and fifth digit, C1, corresponds to the proposed concrete cover of $1d_b$. Thus, the 7 cast beams were grouped in three categories: two were KE1C1, two were FE1C1 and three were IE1C1.

2.3.2 Mechanical properties

Another researcher conducted the material testing of Com K and F design mixes. The compressive strength was determined by testing 150 mm long cylinders with a 75 mm diameter at a loading rate of 1.0 ± 0.05 MPa/s (ASTM C1856 2017) using the Controls Pilot testing machine. The average compressive strength for Com K, In-house and Com F were 122 MPa (at 141 days), 153 MPa (at 152 days) and 128 MPa (at 121 days), respectively. The specimens reached the age of hydration, such that this was not a parameter of this current study. In addition, a four-point loading test was conducted on two sets of prisms (P1 and P2) in accordance with ASTM C1856, (2017) with the exception that the loading rate was reduced and set to 0.005 mm/min to observe a detailed behaviour of the specimens in the MTS universal testing machine. Two sets of prisms were considered: P1 and P2 with nominal cross section of 75 mm x 75 mm, with a span-to-depth ratio of 1 for set P1 (280 mm long) and 2 for P2 (500 mm long). The mid-span deflection was measured using a smaller version of the frame chord system previously described in Section 2.2. The flexural behaviors of the In-house mix are presented in Figure 7 where P1 and P2 consisted of three and two prisms, respectively.

For the set P1, the average flexural tensile strengths were 23 MPa, 28.8 MPa and 31.9 MPa with an average peak mid-deflection of 0.64 mm, 0.56 mm and 1.235 mm for Com K, In-house and Com F, respectively. For the set P2, the average flexural strengths were 24.9 MPa, 27.5 MPa and 36.2 MPa with an average peak mid-deflection of 1.68 mm,1.23 mm and 2.5 mm for Com K, In-house and Com F, respectively.

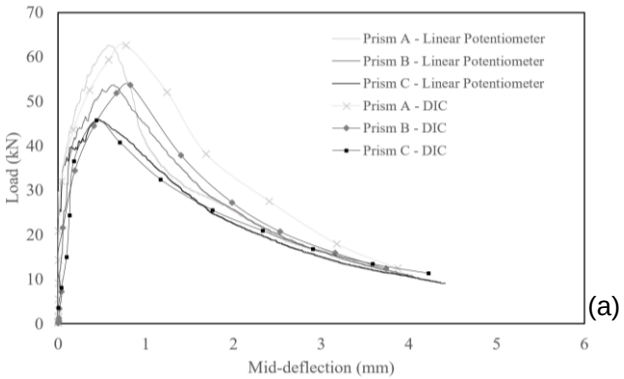

(a)

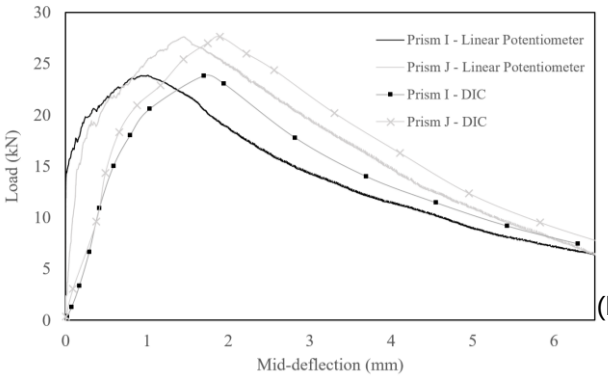

(b)

Figure 7: Results of set (a) P1 (280 mm) and (b) P2 (500 mm)

3 RESULTS AND DISCUSSION

3.1 Global behaviour and mode of failure

Figure 8 presents the load versus mid-span deflection as measured by the linear potentiometer and predicted using the DIC for the three design mixes for a concrete cover of $1d_b$ and embedment length of $5d_b$. The peak load and the mid-span deflection are directly proportional to the flexural tensile strength of the material. The peak load and mid-span deflection are 72.4 kN and 1.6 mm respectively for Com K, 81.2 kN and 2 mm respectively for the In-house mixture, and 96.5 kN and 3.1 mm respectively for Com F. All three materials have the same pre-peak ascending response, yet vary widely in the post-peak descending response. The high flexural tensile strength of mix Com F leads to more ductile curves with a higher energy dissipation capacity to carry greater loads for the same mid-span deflection. For an applied load of 25 kN, the mid-span deflection on the descending branch was 10.4 mm for KE1C1, 12.5 mm for IE1C1 and 25.3 mm for FE1C1. The Digital Image Correlation tool predicts similar results to the observed deflections, yet it slightly underestimates the initial stiffness and slightly overestimates the deflections.

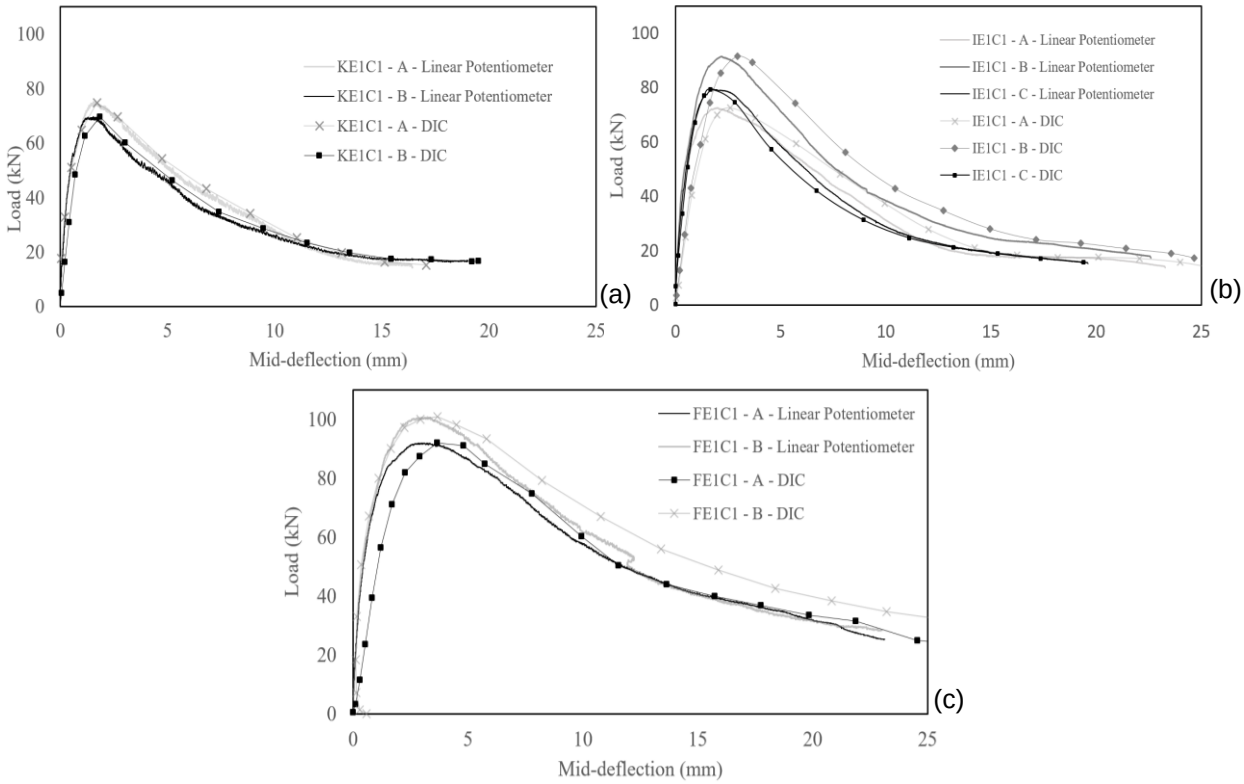

Figure 8: Load vs. mid-span deflection for a concrete cover equal to $1.0d_b$ and an embedment length equal to $5d_b$ (E1C1) for (a) Com K, (b) In-house and (c) Com F

The auxiliary bars were positioned to not interfere in the bond response of the main 15M test bar. The bond depends mainly on the concrete flexural tensile strength as previously described in Section 2.3.2. By approximating the bond stress distribution as uniform along the short embedment length, the average peak bond strength calculated based on Equation (1) was 23.4 MPa for Com K with a slip of 0.42 mm, 26.2 MPa and a slip of 0.76 mm for the In-house mixture, and 31.2 MPa with a slip of 1.58 mm for Com F. The experimental average bond stress slip responses presented in Figure 9 follow the same behaviour for all the specimens starting with a high initial stiffness and reaching a high average bond strength at a slip of 0.5-1 mm. Slip of the reinforcing bar occurs when the predominant splitting crack at the bottom face was created in the post-peak phase. For a 25 kN load, the slip in the post-peak response is 7.3 mm for the Com K concrete, 8.5 mm for the In-house design mixture, and 15.5 mm for the Com F concrete.

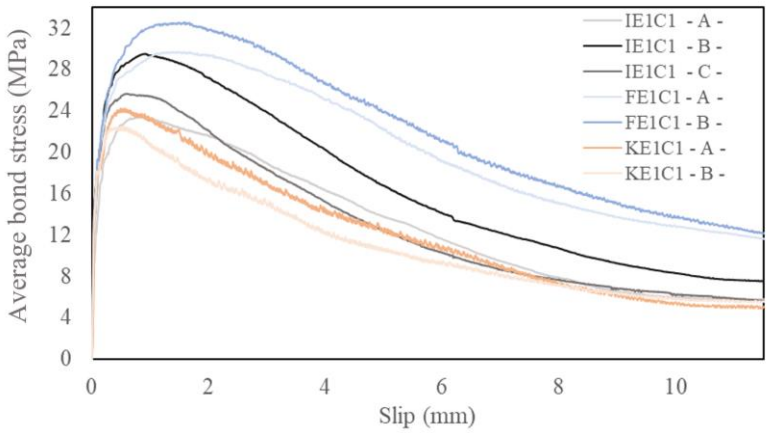

Figure 9: Experimental average bond stress slip response for the three design mixtures

3.2 Failure mode

The first crack for all specimens initiated near the notch at 70-75% of the peak load indicating the high tensile strength of all design mixes. These associated mid-span deflections were minimal indicating a highly ductile material with a large initial stiffness. An increase of the applied load propagated the cracks near the notch upwards towards the compression zone as shown in Figure 10 (a, c and e). For all the 7 specimens, before reaching the peak load, one narrow splitting crack was visually detected in the bottom cover starting from the loaded end of the bar extending to the end of the embedment length. Moreover, the steel fibers were able to bridge across the bottom splitting crack preventing its opening. After the development of the first splitting crack, additional transverse cracks spread due to the pullout of the reinforcing bar. This was accompanied by a gradual reduction of the load emphasizing the role of the steel fibers to bridge across the cracks, eliminating any brittle mode of failure. The beams with the Com K mix clearly failed in a pullout-splitting mode as shown in Figure 10 (b). Regarding the In-house design mixture, IE1C1A developed a splitting crack, IE1C1B presented a cone failure, and IE1C2C failed by a V-type split as shown in Figure 10 (d). Specimen FE1C1A of the Com F mix failed by pullout-splitting, while specimen FE1C1B developed a splitting crack with a half V-type split as shown in Figure 10 (f). Thus, it is apparent that the high strength and deformation capacity of steel-fibre-reinforced concrete can alter dramatically the mode of failure from pullout-splitting to the cone and V-type splitting failures.

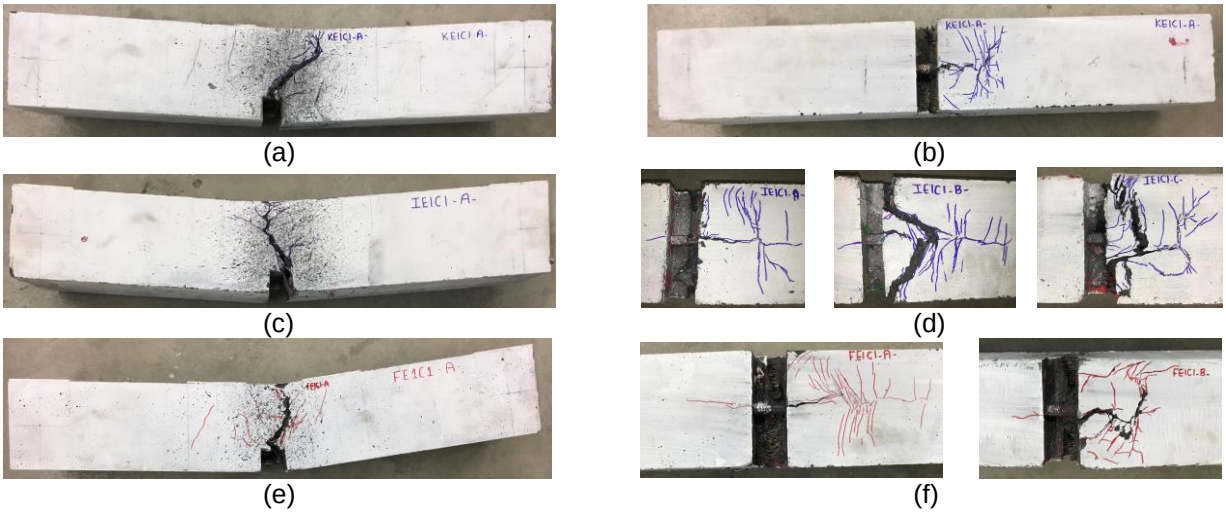

Figure 10: (a) Side face Com K at failure, (b) bottom face Com K at failure, (c) side face In-house at failure, (d) bottom faces In-house at failure, (e) side face Com F and (f) bottom faces Com F at failure

Table 2 presents a summary of the mid-span deflection ($\Delta_{1^{st}\,cr}$) generated by the load at first crack ($F_{1^{st}\,cr}$); the maximum peak load (F_{peak}) and the corresponding mid-span deflection (Δ_{peak}); the maximum bar stress (f_s), the average bond strength (f_b), the slip for the maximum average bond stress (slip), the deflection of the beam ($\Delta_{P=25kN}$) and the slip of the reinforcing bar ($slip_{25kN}$) when the load drops to 25 kN in the post-peak phase; and the mode of failure. Based on the cracking pattern and the reinforcing bar state, several modes of failure were detected. Each mode is characterized by a letter where C, V, P-S, P-S/V, depicts cone, v-type split, pullout-split, and v-type split with pullout, respectively.

From Table 2, the 15M steel bar yielded for the Com K and In-house design mix specimens. The reinforcing bars for the Com F specimens attained their nominal ultimate tensile strength. A concrete cover of $1d_b$ with an embedment length of $5d_b$ was sufficient to provide the necessary confinement to reach the ultimate bond strength for all three mixes.

Table 2: Summary of salient parameters from beam tests

Beam	$F_{1^{st}\,cr}$ (kN)	$\Delta_{1^{st}\,cr}$ (mm)	F_{peak} (kN)	Δ_{peak} (mm)	f_s (MPa)	f_b (MPa)	Slip (mm)	Δ_{25kN} (mm)	$Slip_{25kN}$ (mm)	Failure mode
KE1C1A	53.5	0.6	75.1	1.62	485.0	24.3	0.56	10.54	7.41	P-S
KE1C1B	48.8	0.5	69.7	1.54	449.8	22.5	0.52	10.32	7.11	P-S
FE1C1A	66.4	0.8	92.1	2.96	> fu	29.7	1.39	23.35	12.04	P-S
FE1C1B	75.7	1.0	101.0	3.24	> fu	32.6	1.58	27.21	19.00	P-S/V
IE1C1A	54.4	0.6	72.6	2.00	468.1	23.4	0.81	11.37	7.80	P-S
IE1C1B	68.6	0.9	91.5	2.17	590.6	29.5	0.89	14.80	10.25	V
IE1C1C	58.0	0.7	79.5	1.78	513.3	25.7	0.58	11.36	7.52	C

4 CONCLUSION

This experimental research program provides valuable results for the international bond databank which may be used in the future to corroborate numerical and analytical models being developed for future enhancement of design codes, specifically targeting the use of Ultra-High-Performance Concrete (UHPC) in structural design. Bond-slip results extracted from the experiments may be used in the calculation of the development length of reinforcing bars in Ultra-High-Performance Steel Fiber Reinforced Concrete (UHP-SFRC) such as embedment, anchorage, and lap-splice lengths. The high tensile strength of UHP-SFRC permits reduced reinforcing bar embedment lengths and therefore facilitate the design of more complex structural systems. This study illustrates that a concrete cover of $1d_b$ with an embedment length of $5d_b$ is sufficient to yield a reinforcing bar with a nominal yield strength of 400 MPa.

Acknowledgments

The authors would like to acknowledge concrete producing companies that have donated prepackaged UHPC mixes, and also Stoney Creek Norchem, and BASF for their generous donations of the materials needed for this study.

References

ACI Committee 408. 2003. ACI 408R-03 Bond and Development of Straight Reinforcing Bars in Tension. *American Concrete Institute*, Farmington Hills, MI.

Alford, N. McN, G. W. Groves, and D. D. Double. 1982. Physical Properties of High Strength Cement Pastes. *Cement and Concrete Research,* **12**(3): 349–358.

ASTM C230/C230M-14. 2014. Standard Specification for Flow Table for Use in Tests of Hydraulic Cement. *American Society for Testing and Materials*, West Conshohocken, PA.

ASTM C1856/C1856M-17. 2017. Standard Practice for Fabricating and Testing Specimens of Ultra-High Performance Concrete. *American Society for Testing and Materials*, West Conshohocken, PA.

Bache, H.H. 1981. *Densified Cements Ultra-Fine Particle-Based Materials,* 2nd International Conference on Superplasticizers in Concrete, Ottawa, Canada, 33

Doiron, G. 2017. UHPC Pier Repair / Retrofit Examples of Completed Projects in North America. *AFGC-ACI-Fib-RILEM Int. Symposium on Ultra-High Performance Fibre-Reinforced Concrete*, Montpellier, France, **1**: 983-992.

Gürkan, Y.; Ş. Mustafa; A. Özgür. 2018. 15 - *Engineered Cementitious Composites-Based Concrete*. *Eco-Efficient Repair and Rehabilitation of Concrete Infrastructures*, Elsevier, 387–427.

Haber, Z. B., I. De la Varga, B. A. Graybeal, B. Nakashoji, R. El-Helou. 2018. *Properties and Behavior of UHPC-Class Materials*, FHWAHRT-18-036, Federal Highway Administration, Washington, DC.

Lagier, F.; B. Massicotte, and J. P. Charron. 2016. Experimental Investigation of Bond Stress Distribution and Bond Strength in Unconfined UHPFRC Lap Splices under Direct Tension. *Cement and Concrete Composites*. **74**: 26-38.

Lankard, D. R. 1985. Slurry Infiltrated Fiber Ccncrete (SIFCON). *Concrete International,* **6**(12): 44-47.

Li, V. C., and C. K. Y. Leung. 1992. Steady-State and Multiple Cracking of Short Random Fiber Composites. *Journal of Engineering Mechanics*, ASCE, **118**(11): 2246-2263.

Mehta, P. K. and R. W. Burrows. 2001. Building Durable Structures in the 21st Century. *Concrete International,* **23**(3): 57-63.

Naaman, A. E., and H. W. Reinhardt. 2003. High Performance Fiber Reinforced Cement Composites HPFRCC-4: International RILEM Workshop. *Materials and Structures*. **36**(10): 710-712.

Richard, P., and M. Cheyrezy. 1995. Composition of Reactive Powder Concretes. *Cement and Concrete Research,* **25**(7): 1501–1511.

Ronanki, V.S., D.B. Valentim, and S. Aaleti. 2016. Development Length of Reinforcing Bars in UHPC: An Experimental and Analytical Investigation. *First International Interactive Symposium on UHPC,* Des Moines, IA, **4**: 1-9.

Roy, D. M., G. R. Gouda, and A. Bobrowsky. 1972. Very High Strength Cement Pastes Prepared by Hot Pressing and Other High Pressure Techniques. *Cement and Concrete Research*. **2**(3): 349-366.

Schoening, J., and J. Hegger. 2012. Lapped Splices in UHPC Joints. *4th* International Symposium *Bond in Concrete: Bond, Anchorage, Detailing,* Brescia, Italy, **2**: 687- 694.

Shao, B. 2016. Mix Development of PLC-Based Ultra-High Performance Fibre Reinforced Concrete and Characterization of Key Mechanical Properties and Time-Dependent Behaviour. *MaSC. Thesis,* University of Toronto*,* 1-130.

Tastani, S. P., and S. J. Pantazopoulou. 2010. Direct Tension Pullout Bond Test: Experimental Results. *Journal of Structural Engineering,* **136**(6): 731–743.

Tastani, S. P., M. S. Konsta-Gdoutos, S. J. Pantazopoulou, and V. Balopoulos. 2016. The Effect of Carbon Nanotubes and Polypropylene Fibers on Bond of Reinforcing Bars in Strain Resilient Cementitious Composites. *Frontiers of Structural and Civil Engineering*. **10**(2): 214-223.

Vitek, J. L., R. Coufal, and D. Čítek. 2013. UHPC - Development and Testing on Structural Elements. *Procedia Engineering*, **65**: 218-223

White, D. J., W. A. Take, and M. D. Bolton. 2003. Soil Deformation Measurement Using Particle Image Velocimetry (PIV) and Photogrammetry. *Géotechnique*, **53**(7): 619-631.

Yudenfreund, Marvin, Ivan Odler, and Stephen Brunauer. 1972. Hardened Portland Cement Pastes of Low Porosity I. Materials and Experimental Methods. *Cement and Concrete Research*, **2**(3): 313-330.